THE INFLUENCE OF ROTATION AND BUOYANCY ON RADIALLY INWARD AND OUTWARD DIRECTED FLOW IN A ROTATING CIRCULAR COOLANT CHANNEL

M. Elfert H.Hoevel K.Towfighi

DLR
Deutsche Forschungsanstalt für Luft- und Raumfahrt
(German Aerospace Research Establishment)
Institute of Propulsion Technology
51140 Cologne (Germany)

Abstract

The buoyancy and rotation influence on the development of a pressure-driven air flow in a circular-sectioned coolant channel is presented in this paper. The channel is rotating about an axis perpendicular to its own centerline with an eccentric orientation like in turbine blade cooling. The two basic cases of radially inward and outward directed flow have been investigated. The flow field of the duct is investigated by means of experiments and numerical calculations to demonstrate rotation effects under both isothermal and heated flow conditions. Coriolis forces generate two counter-rotating vortices in the flow. Distortion of velocity distribution and turbulence intensity arises with increasing rotation. The kidney-shaped displacement of fluid with higher velocity from the core towards the pressure side of the duct leads to drastically diminished shear stresses at the suction while on the remaining of the duct the gradients are enhanced above the nonrotating values. In the presence of density variations across the channel induced by thermal fluxes, buoyancy forces arise significantly influencing the velocity wall gradients and the turbulence levels. Flow visualizations by the oil flow technique and a newly developed camera monitoring of the secondary flow structure were conducted within the rotating channel. Nonintrusive flow measurements were performed with an advanced Laser-2-Focus velocimeter (L2F). Numerical flow simulations were done with a 3D Navier-Stokes flow solver. The experimental data help to understand the Coriolis and buoyancy force affected flow phenomena and provide test data for the validation of numerical flow predictions.

Introduction

The requirements for high-performance and high-efficiency turbomachines demand the optimization of all turbomachinery components to cope with the increase in heat and pressure load as well as to meet the obligatory safety requirements. In the case of turbine blade cooling, it is known that strong centrifugal forces (up to 50,000 g) and Coriolis forces cause a complex flow structure in the coolant flow. Rotation, through Coriolis interaction, generates a symmetric pair of secondary vortices that are streamwise oriented. The change in friction caused by the secondary motion influences heat transfer and pressure drop. Detailed knowledge of the rotational effects on fluid motion as well as local information about heat transfer rate in this situation will help to achieve precise predictions during the design phase that are essential for the development of more sophisticated blade cooling arrangements. A typical view of a cooled turbine blade and a sketch of the flow pattern inside an idealized duct of one of the internal passages is shown in Fig. 1. Several publications [1-6] describe the effect of rotation on heat transfer in cooling channels of different shapes, but regarding experiments on the flow field in rotating passages only a few investigations [7-10] can be found due to the difficulty of measurements. The work of Moore [7] shows the secondary flow velocities measured by a hot wire probe in a rectangular duct, but at a low rotational speed. However, all investigations are limited to isothermal flows without the added complexity of buoyancy.
Without any heat input from the wall only pure Coriolis influence is prevailing because no density and centrifugal force variations arise in that case. To

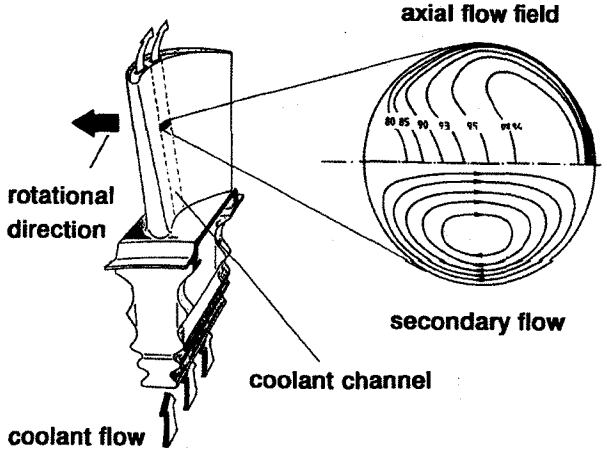

Figure 1: Typical View of a cooled turbine blade and flow pattern in a cross-section of a cooling channel

study the fundamental flow phenomena in more detail, especially in the vicinity of the wall, for the first time *nonintrusive* flow measurements in a narrow rotating duct were done providing information about the turbulence intensities and the velocity field, also with buoyancy imposed.
A numerical method has been developed to calculate the flow and heat transfer in rotating cooling channels of turbine blades [11-13]. To verify the predicted data, experiments on flow visualization and detailed flow field measurements, presented hereafter, were conducted at DLR [14-16].

Test facility

A large-scale coolant duct with a circular cross-section rotating spanwise was chosen for the experiments to ease the experimental work. Air is supplied in the rig through a rotary sealing assembly, a second one is used for venting after the air has passed through the test section. Both are mounted to the end of the double hollow shaft. A schematic of the test rig is given in Fig. 2.

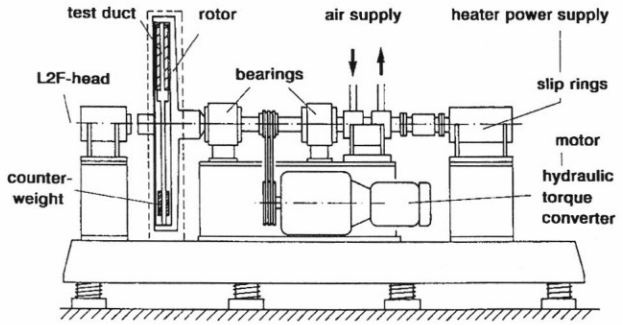

Figure 2: Schematics of the test rig

The pipe diameter *d* of the test duct is 16 mm with a length-to-diameter ratio *l/d* of 20. The dimensionless eccentricity at mid span *E=e/d* is about 20. It should be noted, however, that eccentricity and flow direction are irrelevant for isothermal flow because Coriolis forces depend only on angular and throughflow velocity. Flow rate, spin rate, and pressure level can be individually adjusted.

Flow visualization

To analyze the rotational flow phenomena, several kinds of flow visualization techniques have been applied. Using the oil flow visualization method, wall streamline patterns could be achieved within the rotating duct. The duct wall has been previously painted with a mixture consisting of oil of appropriate viscosity, oil acid and as contrast pigment TiO_2 and has been then exposed to the rotational flow for a time that should be long enough to let the oil paint getting dry. Figure 3 shows the streamline patterns on the inner duct wall. The duct is dividable in two halves and is opened after the test run. The vortex affected streamlines run from the pressure side (top and bottom) to the suction side (center) and show clearly the inclination of the boundary layer flow direction against the pipe axis of about 8°. The pattern in Fig. 3 is formed at a Reynolds number of 45,000 and a rotation number of 0.05 with the flow direction to the right.

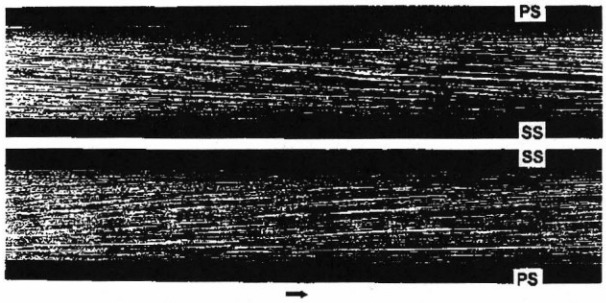

Figure 3: Oil flow visualized wall streamline pattern of a rotating duct (Re=45000, Ro=0.05)

To obtain more information of the vortex behaviour within the cross-section, a co-rotating video system has been installed downstream, viewing inside the duct. A perspex ring allowed the lighting of a cross-section by a laser light sheet. The laser light is guided into the rotating system via the same optical unit used for the laser flow measurements. In order to visualize the vortex flow structures, seeding of the boundary layer with oil droplets is provided by a particle generator. To avoid complete mixing of the oil fog with the air flow, seeding is done a small distance of 10 pipe diameters upstream of the observed area via an extra supply line guided through the shaft. The set-up of the flow visualization technique is shown in Fig. 4. The video signal is transferred to a recording system via normal slip rings. With frame grabbing on a PC-machine the video pictures can be captured. The digetized pictures have been improved with re-

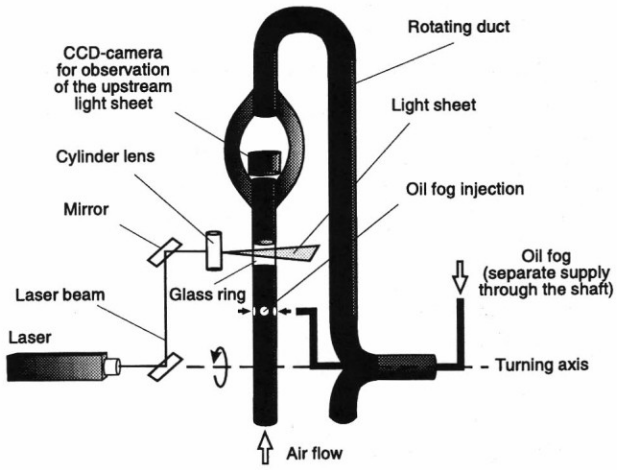

Figure 4: Set-up of vortex flow visualization using a co-rotating camera system and oil fog seeding

gard to luminance and brightness. A set of pictures at different rotation numbers demonstrate clearly the vortex shapes, driving to the side walls with increasing angular velocity. Although this visualization technique is restricted to laminar flow situation, the main effects are also present and can be studied. In Figure 5 are pictures included for a throughflow Reynolds number of 1500 with the rotation numbers in the 0.06 to 0.6 range. With a higher angular velocity the vortices are suppressed to the side walls and no seeded boundary layer material is found in the flow core.

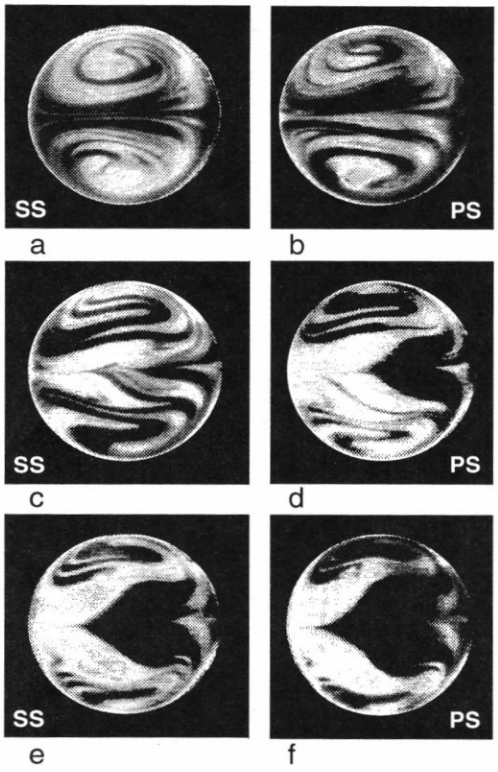

Figure 5: Secondary vortex structures for laminar flow at Re=1500 and different rotation numbers
a) Ro = 0.06, b) Ro = 0.12, c) Ro = 0.24,
d) Ro = 0.36, e) Ro = 0.48, f) Ro = 0.6

Optical measurements of flow quantities

For the nonintrusive measurement of flow velocities, angles and fluctuations inside the rotating duct the Laser 2 Focus (L2F) technique [17,18] has been applied using a newly developed optical unit to direct the two laser beams into the rotating frame of reference [19]. The optical L2F device mounted in front of the rotor enables the system to stationary non-triggered signal processing. Figure 6 shows a schematic drawing of the optical set-up used in this kind of application.

Following the beam path from the laser to the probe volume, the laser light is emitted by an Ar^+ ion laser of 4 Watt power output which is connected to the launching unit mounted to the test rig by an optical fibre for vibration decoupling purpose. In this unit, the laser beam is split into two beams. The rotation prism co-rotating with half the speed of the rotor focuses the two beams in the rotating frame of reference, saving invariable orientation of the light barrier in relation to the rotating duct. From the turning axis the beams are guided by several mirrors to the measuring point inside the duct finally passing a plane optical window in the duct wall. Adjustment of the mirrors enables flow measurements at different circumferential and axial duct locations. The two beams are highly focused in two foci (measuring volume) by means of a traversable focus lens mounted to the rotor. Traversing of the lens, which is also possible during rotation, moves the probe volume within the test section along a radius. Measurements were taken on the opposite half of the duct to avoid influence of the wall shape on the flow near the window.

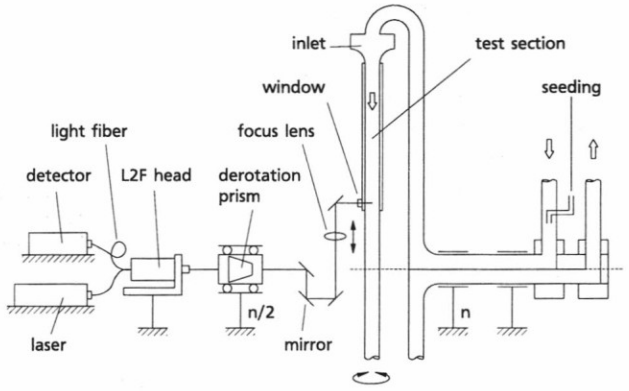

Figure 6: Optical set-up of the laser measuring equipment for the nonintrusive flow measurements

The L2F method is based on time of flight measurements of co-flowing particles. Small oil droplets with a size less than 0.5µm were added to the flow before entering the shaft. The flow-following behaviour of these particles even at high accelerations has been successfully demonstrated and thereby a correlation between particle and flow velocity is assured. The passing of a particle conveyed by the flow through the light barrier (i.e. the 2 foci) produces two consecutive light pulses. The time interval between the signals and the known distance of the foci give the flow velocity. The light pulses received by the same optic in the outer area - the inner part is used for launching the beams - are imaged at two photo multipliers each assigned to a beam in the probe volume.

The flow angle is detected by changing the orientation of the light barrier. Due to the 2D-technique and the radial adjustment of the beams, only circumferential flow angle can be measured. In the plane normal to the direction of rotation, where secondary flow is almost parallel to the wall, angle determination produces true flow angle, while in the plane of rotation from suction to pressure side secondary flow is directed normal to the wall. No deviation from the throughflow direction measured in this case confirms the expected line of symmetry in the vortex pattern.

For both velocity as well as angle determination, some thousands of time of flight measurements are recorded. The measured data result in frequency distributions from which a statistical mean velocity, degree of turbulence, and flow direction are evaluated. The closest distance to the wall achieved was 0.1 mm.
Figure 7 shows the test pipe with an inlet settling chamber containing flow straighteners such as impingement plate, honeycombs, and several meshes which should mainly break up incoming vorticity from the upstream conduit where flow is already exposed to rotational forces.

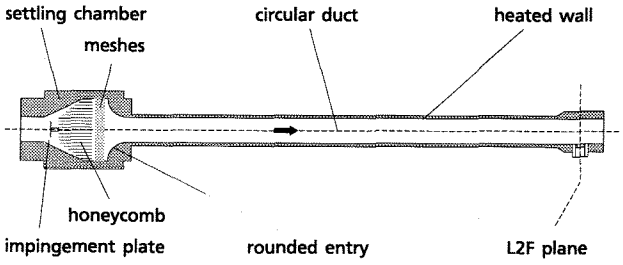

Figure 7:Test duct for flow measurements

The experimental uncertainty inherent in the L2F-measurement technique was investigated in detail by Schodl [20]. Among other things it depends on the particle concentration in the measuring volume. In the boundary layer flow the signal rate slows down increasing the signal to noise ratio. Therefore the uncertainties in the velocity and turbulence evaluation are in-between $\leq \pm 0.5$ % in the core flow and $\pm$ 3.0 % close to the wall. Angle determination uncertainty ranges between $\pm$ 0.2° and $\pm$1.0°, respectively. Mass flow rate, heat flux, temperatures, pressures and speed have been measured with an accuracy of $\pm$1%.
The measuring geometry in relation to the direction of rotation, both radially inward as outward, within the cross-section of the duct is described by Fig. 8 where

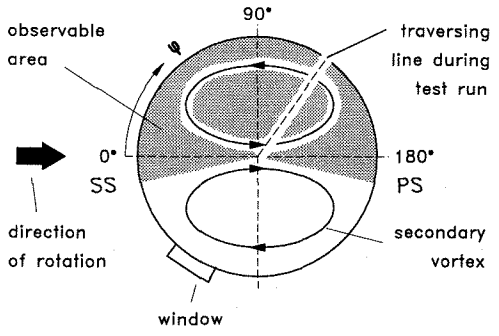

Figure 8:Measuring plane across the duct with circumferential angle definition

the circumferential angle φ of the duct is defined with φ = 0° at the suction side (SS) and φ = 180° at the pressure side (PS). In the following figures radial traversing is done along a line coinciding with the direction of rotation φ = 0° and 180° and normal to that φ = 90°.

Results and Discussion

Coriolis influence on isothermal flow

The tests under isothermal conditions disclose the Coriolis induced rotational effects. For different rotation numbers the flow is analyzed in the following figures with the non rotating case for comparison purpose. After passing the plenum with an area contraction of 10 and rounded entry, the flow is developing downstream in the test duct. L2F measurements were conducted after a duct length x/d of 20 at an actual eccentricity E of 10. Velocity is related to the bulk mean velocity evaluated via integration of field data, otherwise obtained from mass flow and actual pressure.
Rotational parameters appear as additional source terms in the momentum equations. For instance, one equation in dimensionless form for the x-direction (throughflow direction) is given below showing the Coriolis and buoyancy terms beside the ordinary convection, pressure, and diffusion term for rotating duct flow:

$$\underbrace{U\frac{\partial U}{\partial X}+V\frac{\partial U}{\partial Y}+W\frac{\partial U}{\partial Z}}_{\text{Convection}} = \underbrace{-\frac{\partial P}{\partial X}}_{\text{Pressure}} + \underbrace{\frac{1}{Re}\left[\frac{\partial^2 U}{\partial X^2}+\frac{\partial^2 U}{\partial Y^2}+\frac{\partial^2 U}{\partial Z^2}\right]}_{\text{Diffusion}} \underbrace{-2\cdot Ro\cdot V}_{\text{Coriolis}} \underbrace{-E\cdot Ro^2}_{\text{Centrifugal}} \underbrace{-\frac{Gr}{Re^2}\Theta}_{\text{Buoyancy}}$$

The basic dimensionless fluid governing parameters appear in this equation as the Reynolds number, *Re*, the rotation number, *Ro*, and the buoyancy parameter, Gr/Re^2 which can be expressed as:

$$Gr/Re^2 = (\Delta\rho/\rho)\ E\ Ro^2,$$

and the eccentricity ratio *E*. Secondary motion depends on the ratio of Coriolis forces to viscous forces which can be seen by an analysis of dimensions which exhibits that Coriolis effects would be best correlated by the rotational Reynolds number Re_{rot}. The rotational Reynolds number is dependant only on the angular velocity Ω as primary variable rather than flow velocity u ($Re_{rot} = Ro\ Re$).

$$\frac{Coriolis\ forces}{viscous\ forces} = \frac{\rho\Omega u}{\mu u/d^2} = \frac{\rho\Omega d^2}{\mu} = \mathrm{Re}_{rot}$$

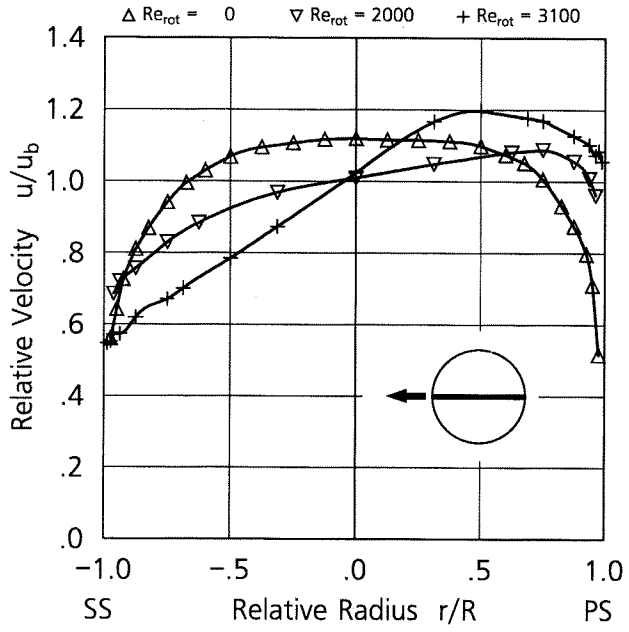

Figure 9: Coriolis influence on axial velocity (SS - PS, Re=45,000)

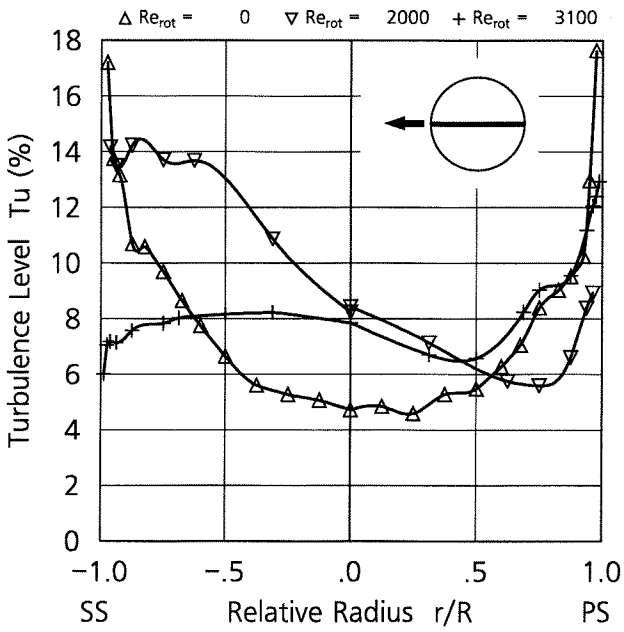

Figure 11: Coriolis influence on turbulence level (SS - PS, Re=45,000)

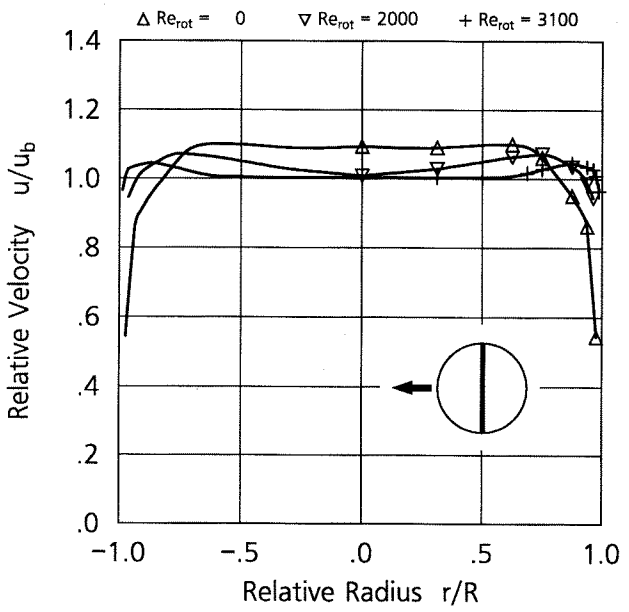

Figure 10: Coriolis influence on axial velocity (φ=90°, Re=45,000)

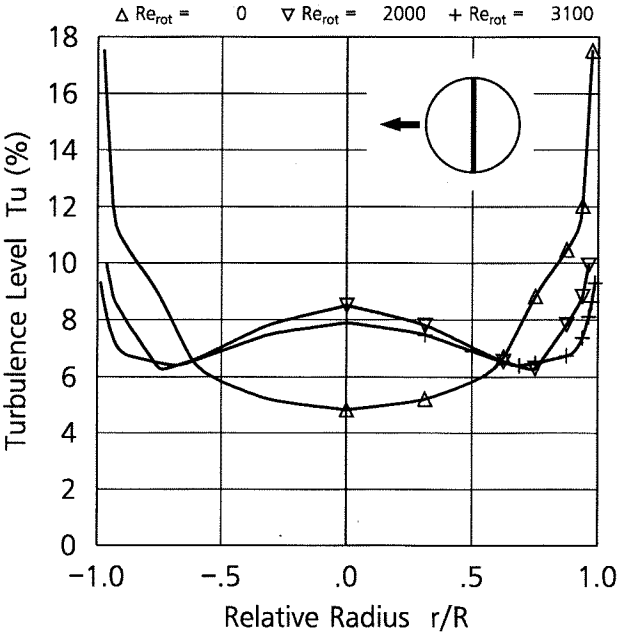

Figure 12: Coriolis influence on turbulence (φ = 90°, Re = 45,000)

The distortion of axial velocity (Fig. 9 and 10) increases with increasing rotational Reynolds number. Secondary vortex generation is caused by the imbalance of pressure forces against Coriolis forces in the boundary layer where the Coriolis forces ($\Omega \cdot u$) diminish due to the wall gradient of velocity. The core of the fluid is shifted to the pressure side due to inertial forces enhancing the velocity gradient there with regard to the non rotating value. A strong depression is formed at the opposite surface, the suction side, becoming deeper with increasing rotation. The Coriolis influence on turbulence intensity (Fig. 11 and 12) reduces turbulence at the pressure side but strongly enhances it in the region of velocity drop near the suction side becoming weakest at the highest rotation number. The magnitude of secondary velocity is measured in this comparison up to 10 percent of axial flow velocity for *Re=45,000* and *Ro=0.045* and *0.07*, respectively (Fig. 13). The center of the vortex cell is identified where the curve is crossing zero line.

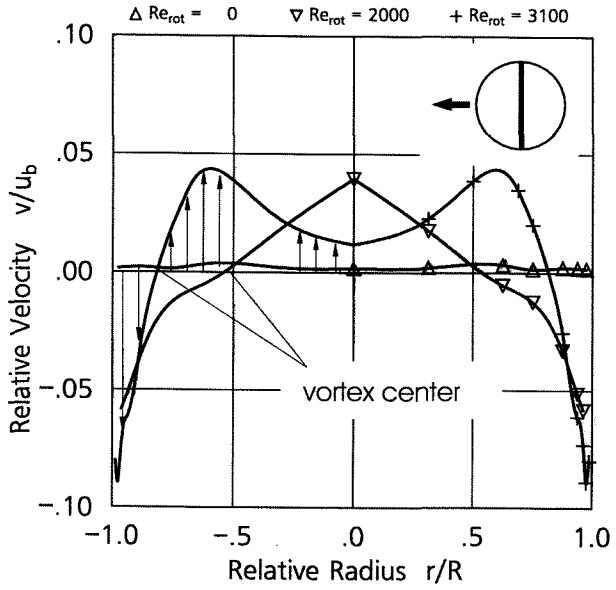

Figure 13: Coriolis influence on secondary flow velocity (φ=90°, Re=45,000)

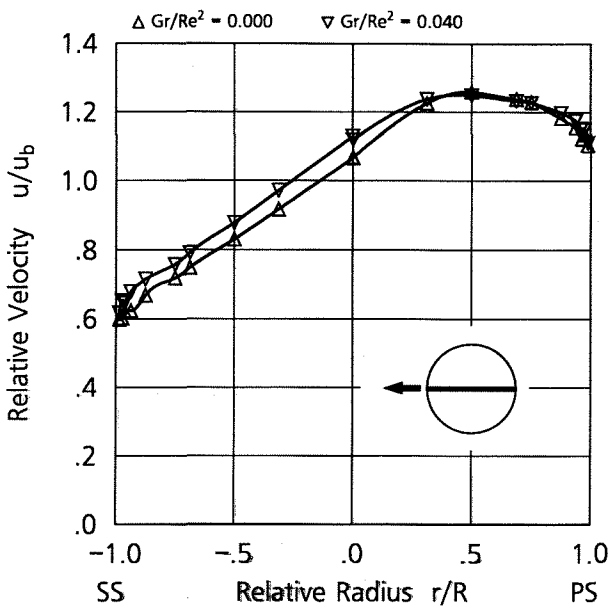

Figure 15: Buoyancy influence on axial velocity with radially inward directed flow
(SS - PS, Re=45,000, Ro=0.08)

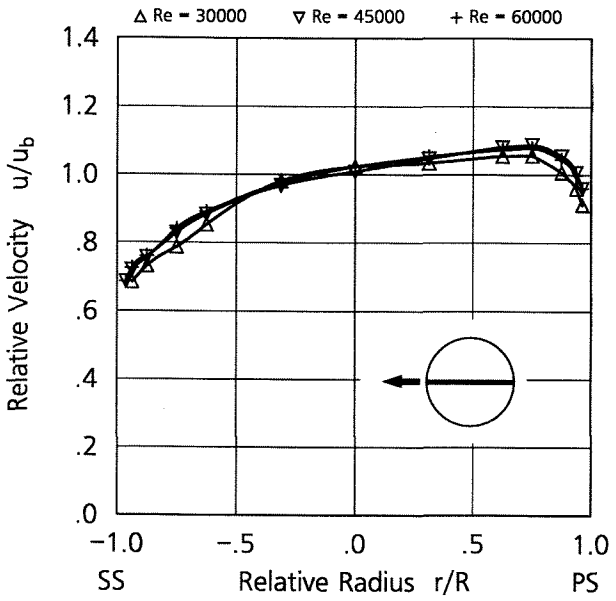

Figure 14: Influence of Reynolds and Rotationnumber on axial velocity at constant speed
(SS - PS, Re=45,000)

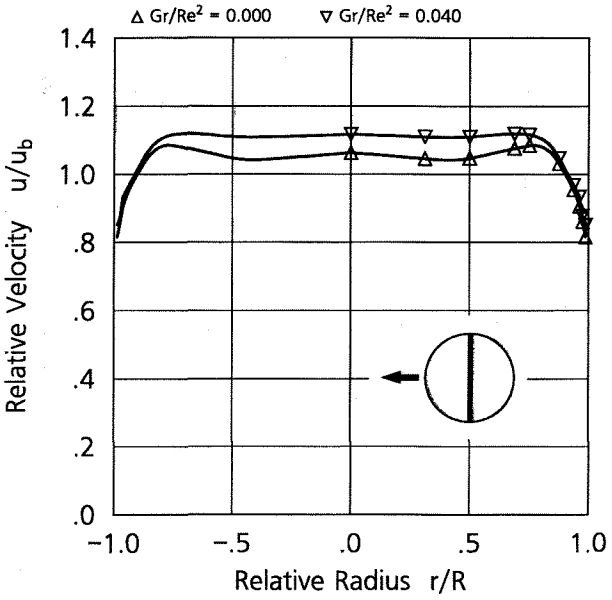

Figure 16: Buoyancy influence on axial velocity with radially inward directed flow
(φ = 90°, Re = 45,000, Ro = 0.08)

Although the streamwise equation of motion shows the Coriolis term *(2 Ro V)* as the principle term which would modify the streamwise velocity distribution, a variation of the rotation number does not exhibit any clear Coriolis effect as it can be seen at the following diagrams. In Fig. 14 the axial velocity ratio is related to the Reynolds number and the rotation number which varies from 0.37 to 0.62 because of the Reynolds number change, keeping the same rotational Reynolds number of 2000, i.e. constant Ω.

Buoyancy influence on radially inward directed, heated flow

Heating of the flow is provided by electrical heater foils of 0.15 mm thickness attached to the wall over

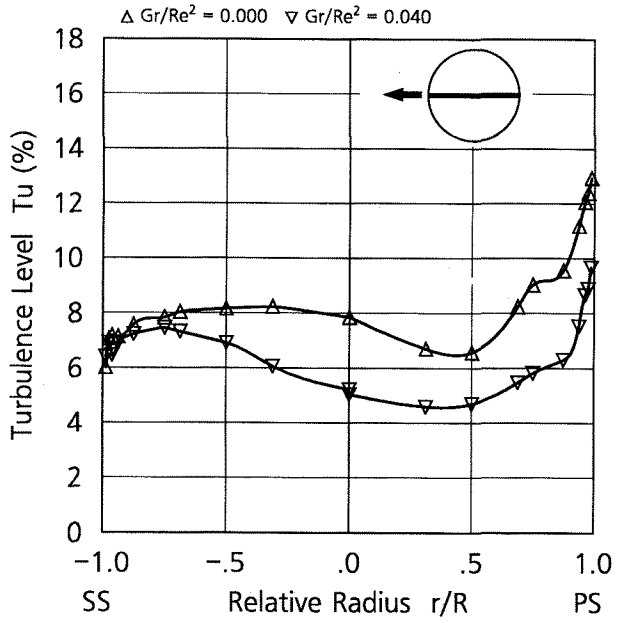

Figure 17: Buoyancy influence on turbulence level with radially inward directed flow
(SS - PS, Re=45,000, Ro=0.08)

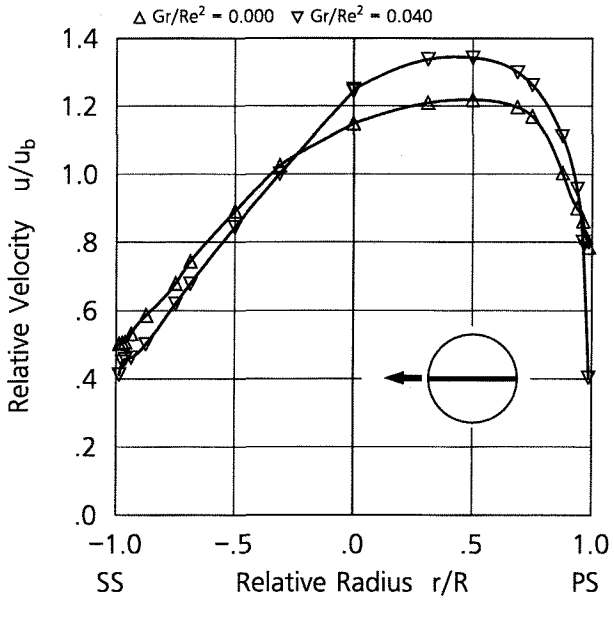

Figure 19: Buoyancy influence on axial velocity with radially outward directed flow
(SS - PS, Re=45,000, Ro=0.08)

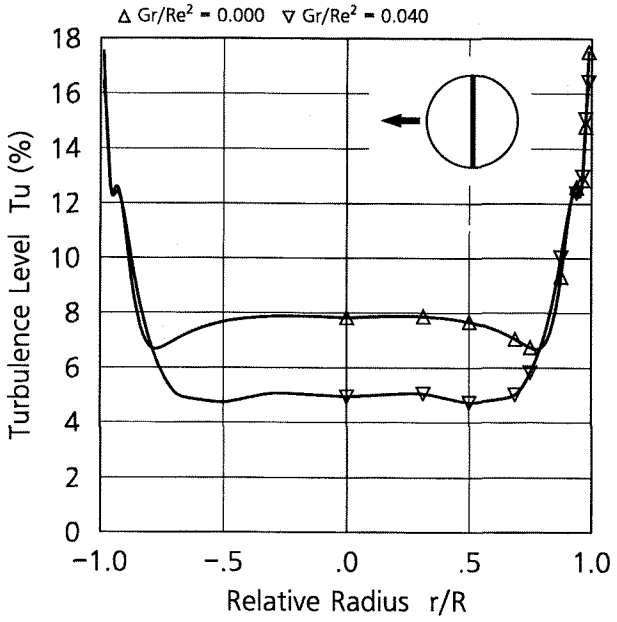

Figure 18: Buoyancy influence on turbulence level with radially inward directed flow
(φ = 90°, Re = 45,000, Ro = 0.08)

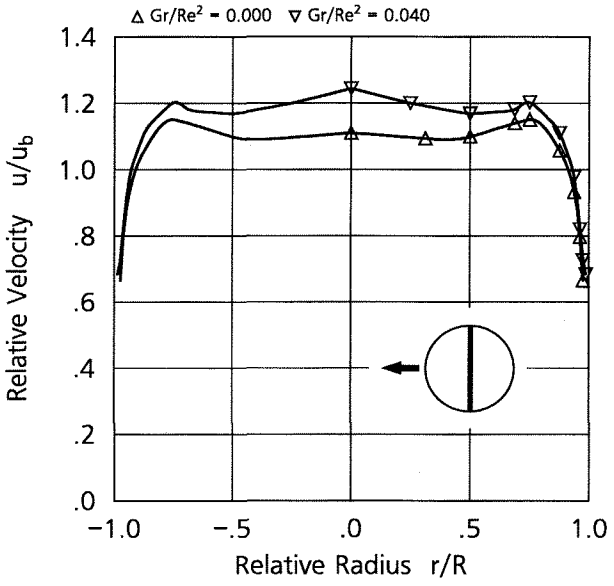

Figure 20: Buoyancy influence on axial velocity with radially outward directed flow
(φ = 90°, Re = 45,000, Ro = 0.08)

an upstream heating length l/d of 16. The flow is directed radially inward, so that buoyancy forces, always centripetal, act in the flow direction. The flow in the rotating duct is 'thermally' as well as hydrodynamically developing and not fully established. The density ratio was evaluated from temperature measurements with $(\Delta\rho/\rho) = (T_w - T_b) / T_b$ to 0.31.
Wall temperature is obtained from the temperature dependency of heater resistance previously calibrated. This yields a buoyancy parameter of 0.04 with a rotation number of 0.08 and a mid span eccentricity ratio of 20.
Figure 15 and 16 show slightly accelerated velocity distributions and Fig. 17 and 18 a significant decrease in the turbulence intensities, especially on the pressure side and in the center-region of the duct, while the other near wall zones remain unchanged.

Buoyancy influence on radially outward directed, heated flow

With turning of the duct and changing the flow direction through the shaft the opposite case has been examined. Mean eccentricity is remained nearly unchanged whereas the actual eccentricity of L2F measurement is now 28.
Figure 19 and 20 show equally slightly accelerated velocity distributions but only in the flow core.
Around the wall the allways centripetal buoyant flow act against the flow and reduces significantly the velocities close to the wall. Fig. 21 and 22 show now an increase in the turbulence intensities, in the center-region of the duct and especially on the pressure side. The adverse buoyant flow forces lead to an overall turbulence level enhancement of about 20% and a very high local value at the pressure side

Numerical flow prediction

As an analytical tool for the investigation of viscous rotational flow effects, a 3D Navier-Stokes code developed by Vogel [11-13] has been used. The governing equations (Reynolds-averaged Navier-Stokes, continuity and energy equations) are numerically solved using a finite volume technique with a cell-centered difference approximation of second order time-accurate explicit three or five step Runge-Kutta algorithm for the time discretization. More stability is gained by using a residual averaging method which can be run either explicit or implicit.The maximal time steps which lead to steady solution are calculated from the CFL-criteria. Eigenvalue scaled scalar artificial dissipation with operators of second and fourth order is added to the numerical scheme to damp out non-physical wiggles produced by the central differencing scheme and to capture physical discontinuities as schocks or strong free shear layers. For three-dimensional subsonic and transonic complex flows with strong physical viscous damping this scheme supplies in a 3D multi-block version acceptable solutions. The rotational fluxes occuring in rotating passages are solved in conservative form.
Turbulence modelling with a Zero-Equation model (i.e. Baldwin and Lomax) neglect free stream turbulence because turbulence is modelled only in boundary layers. In the case of rotational duct flow with strong vortex flows a more complex model is used for turbulence modelling, the Two-Equation k-ε model in low Reynolds form for all y^+. The Two-Equation model is solved using a point implicit solver with first order upwind spatial differences for the convective fluxes producing enough damping and a Red-Black Gauss-Seidel relaxation procedure. Due to the well-known difficulties in solving the source term dominant turbulence equations the scheme is driven up with increasing turbulence production until the full production is reached after several time steps. After this initialization of k and ε the calculation starts with ordinary conditions using the initialized values.

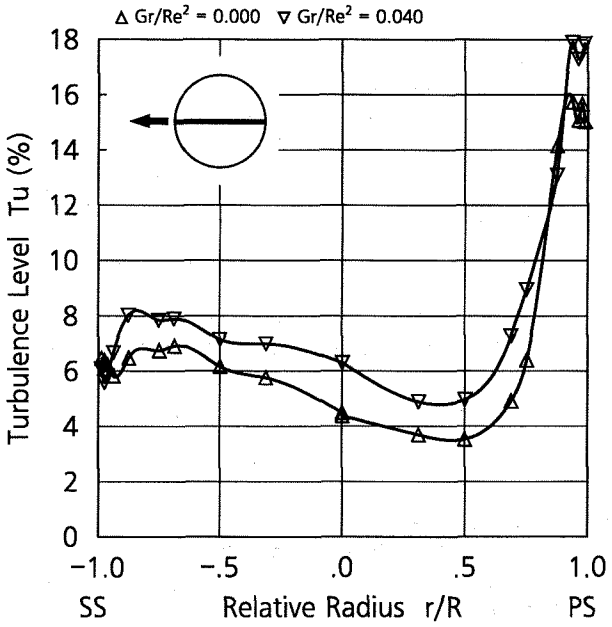

Figure 21: Buoyancy influence on turbulence level with radially outward directed flow (SS - PS, Re=45,000, Ro=0.08)

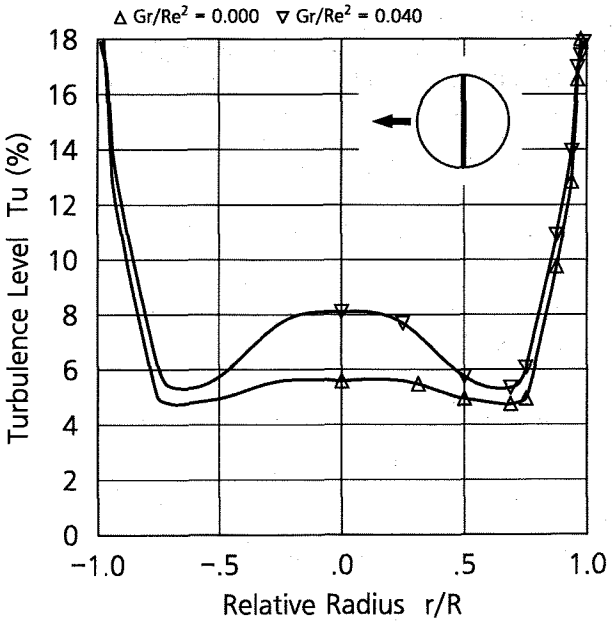

Figure 22: Buoyancy influence on turbulence level with radially outward directed flow(φ = 90°, Re = 45,000, Ro = 0.08)

This code was adapted to cope with rotational duct flow and heat transfer problems. Especially the non-constant boundary conditions in that case due to Coriolis and centrifugal force-effected pressure distributions are to be applied at both sides. The method of pseudo compressibility is used to manage the incompressible flow behavior of the coolant flow. This method using artificial compressibility was pro-

posed by Chorin [22] to achieve an efficient computation compared to the method of solving the poisson's equation for pressure. The method of pseudo compressibility is primarily designed to obtain a steady-state solution of an incompressible flow. The numerical scheme of the compressible Navier-Stokes equations can be easily extended to the incompressible Navier-Stokes equations by adding the time derivative of the pressure to the continuity equation. By introducing a pseudo compressibility, $1/c^2$, into the unsteady, incompressible viscous flow equations, a system of governing equations is formed as follows:

$$\frac{\partial p}{\partial t}\frac{\partial \rho}{\partial p} + \frac{\partial \rho u_i}{\partial x_i} = \frac{1}{c^2}\frac{\partial P}{\partial t} + \frac{\partial \rho u_i}{\partial x_i} = 0$$

The equation differs from the continuity equation for a real compressible flow by the absence of the convective term for the pressure. The absence of this term in the present formulation is an essential feature of this method. Starting from an arbitrary initial condition, the numerical scheme must be chosen such that the solution of the equation for fixed boundary conditions converges to a steady state as the computational progress. When the steady state is approached the effect of the pseudo compressibility diminishes resulting in an incompressible solution. Density change caused by the external heat input is computed via the temperature field got from the solution of the energy equation from a previous iteration step and is taken into account in the buoyancy term.

Validation and results of the numerical scheme

A comparison of calculated and measured velocity (Fig. 23) shows reasonable agreement. This calculation is based on a two-block mesh with 176040 nodes and standard k-ε model.

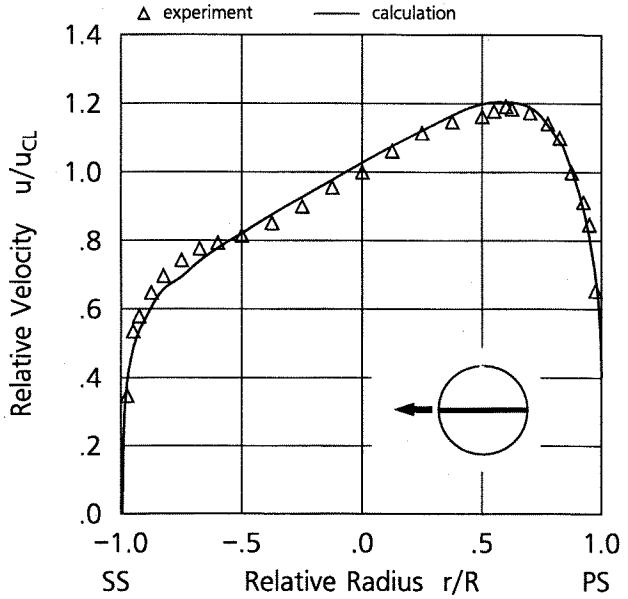

Figure 23: Comparison of measured and calculated velocity distribution (SS-PS, Re= 60,000, Ro= 0.055)

A sketch of the discretized test duct with round entry and a length to diameter ratio of 20 and a view of a cross-section is shown in Fig. 24. The mesh consists of 2 blocks with 176040 nodes.

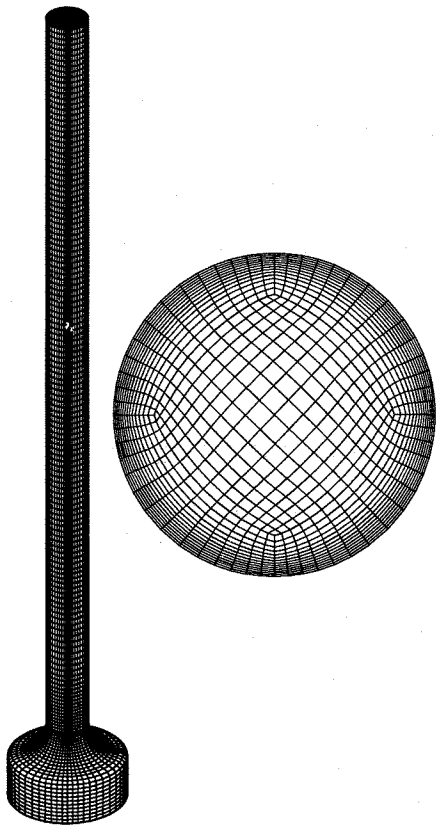

Figure 24: Mesh of test duct with round and a view of a cross-section (2 blocks, 176040 nodes)

The kidney-shaped movement of the fast fluid core to the trailing duct wall is clearly visible by the plotted isolines of axial velocity in Fig. 26 which are a result from computations for two different rotation numbers of 0.4 and 0.8 at a Reynolds number of 45,000. In Fig. 27 velocity vectors are shown in the upper picture and a corresponding streamline plot in the lower for a rotation numbers of 0.4 and a Reynolds number of 45,000.

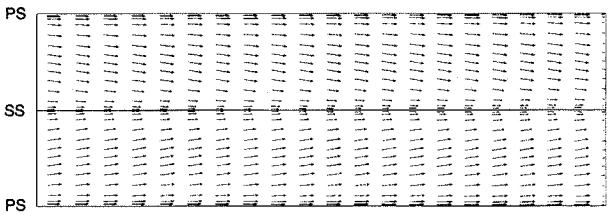

Figure 25: Computed wall velocity vectors and a view of a cross-section (2 blocks, 176040 nodes)

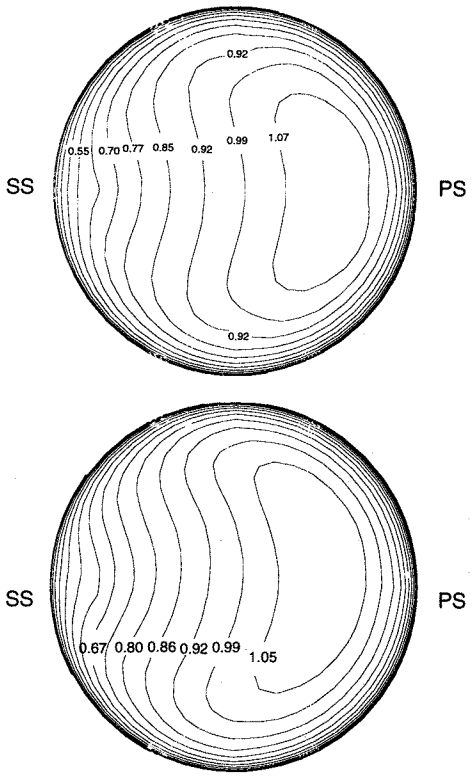

Figure 26: Computed axial velocity distribution (u/u_b) at duct exit for different rotation numbers (Re= 45,000, Ro=0.04 (above), 0.08 (below))

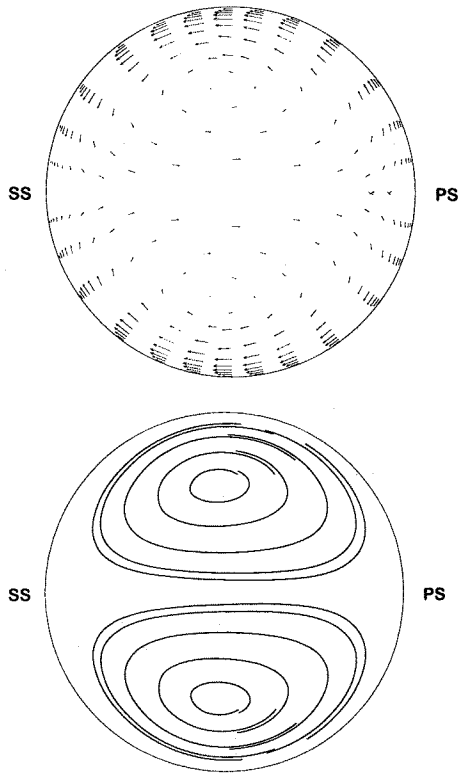

Figure 26: Vortex vectors (above) and corresponding streamlines (below) (Re=45,000, Ro=0.04)

Conclusions

New experimental data are presented in this paper concerning the influence of rotation and buoyancy on the flow in a duct rotating in orthogonal mode with radially inward and radial outward directed flow. From the measurements and the numerical analysis the following phenomena could be stated:

- Flow visualizations of the rotational (isothermal) duct flow verify the presence and magnitude of secondary flow. With the new camera technique, it was possible to monitor the vortex behaviour under laminar flow regime, driving the secondary vortices to both side walls with increasing rotation.
- Nonintrusive flow measurements give precise insights into velocity and turbulence distributions within the developing flow. Distortion of velocity distribution arises with increasing rotation. The kidney-shaped displacement of fluid with higher velocity from the core towards the pressure side of the duct leads to drastically diminished shear stresses at the suction side because of the change of velocity gradients. On the remaining three quarters of the duct circumference the gradients are enhanced above the nonrotating values.
- Buoyancy affects mainly the turbulence intensity in the center region of the duct and the pressure side with a 30% reduction with radial inward flow due to the increase of momentum of heated low density flow mixed to the center by vortex transport mechanisms. However, with radial outward directed flow the opposite effect is observed. The adverse buoyant flow forces lead to an overall turbulence level enhancement of about 20% and a very high local increase at the pressure side.
- The numerical scheme is verified by the experiments regarding the flow field prediction and give detailed insight into the flow development.

Acknowledgements

The authors wish to express their gratitude to Dr. R.Schodl and Mr. M.Beversdorff, DLR, for their support in development and application of the L2F measuring system and Dr.D.T.Vogel for the introduction into the flow solver and

Nomenclature

c	pseudo sound velocity
d	Duct diameter, mm
E	Relative eccentricity, *e/d*
e	eccentricity at mid span, mm
Gr	Grashof number, $\Omega^2 e d^3 \rho \Delta\rho/\mu^2$
k	Kinetic energy of turbulence, m^2/s^2
l	Duct length, mm

p	static pressure
R	Duct radius, m
Re	Reynolds number, $\rho u_h d/\eta$
Re_{rot}	Rotational Reynolds number, $\rho\Omega d^2/\mu$
Ro	Rotation number, $\Omega d/u_h$
r	Radius, mm
T	Temperature, K
Tu	Turbulence level, $\sqrt{u'^2}/u_h$
u,v,w	Velocity in x, y, z-direction, m/s
x	Streamwise coordinate

Greek Symbols

ε	Dissipation rate of k, m^2/s^3
φ	Circumferential angle, deg
μ	Dynamic viscosity, kg/ms
Θ	Temp. ratio, $(T-T_h)/(T_w-T_h)$
ρ	Density, kg/m^3
Ω	Angular velocity, s^{-1}

Subscripts

CL	Centerline
PS	Pressure side
SS	Suction side

References

(1) Morris, W.D. (1981). Heat Transfer and Flow in Rotating Coolant Channels. *Research Studies Press,John Wiley & Sons Ltd.,* Chichester, UK.

(2) Morris, W.D., Ghavami-Nasr,G. (1990). Heat Transfer Measurements in Rectangular Channels with Orthogonal Mode Rotation. *ASME,* Brussels, Begium, Paper 90-GT-138.

(3) Guidez, J. (1988). Study of the Convective Heat Transfer in Rotating Coolant Channel. *ASME J. of Turbomachinery,* **111**, 43-50.

(4) Johnson, B.V., Wagner, J.H., Steuber, G.D., Yeh, F.C. (1992). Heat Transfer in Rotating Serpentine Passages with Trips Skewed to the Flow. *ASME,* Cologne, Germany, Pap. 92-GT-191.

(5) Wagner, J.H., Johnson, B.V., Kopper, F.C. (1991). Heat Transfer in Rotating Serpentine Passages with Smooth Walls. *ASME J. of Turbomachinery,* **113**, No. 3, July 1991, 321ff

(6) Berg, H.P. (1991). Experimentelle Bestimmung des örtlichen inneren Wärmeübergangs von Turbinenleit- und -laufschaufeln mit Hilfe der Analogie zwischen Wärme- und Stoff übergang,. *Ph.D.Thesis,* D17, Tech. Univ. Darmstadt, Germany.

(7) Moore, J. (1967). Effects of Coriolis on Turbulent Flow in Rotating Rectangular Channels. *M.I.T. Gas Turbine Laboratory Report No. 89.*

(8) Hart, J.E.. (1971). Instability and Secondary Motion in a Rotating Channel Flow.*J. Fluid Mech.,* **45**, Part 2, 341-351.

(9) Wagner, R.E., Velkoff, H.R. (1972). Measurements of Secondary Flows in a Rotating Duct. *ASME J. Eng. for Power,* **94**, 261-270.

(10) Johnston, J.P., Halleen, R.M., Lezius, D.K. (1972). Effects of Spanwise Rotation on the structure of Two-Dimensional Fully Developed Turb. Channel Flow. *J. Fluid Mech.*, **46**, Part 3, 533-557.

(11) Vogel, D.T. (1993). Navier-Stokes Calculations of Turbine Flows with Heat Transfer and Film Cooling. *Int. Symposium 'Gas Turbine and Gas Cycle Plants'*, Bled, Slovenia.

(12) Vogel, D.T. (1994). Navier-Stokes Calculations of Turbine Flows with Film Cooling. *19. AIAA-Conference,* ICAS-paper 94-253.

(13) Vogel, D.T. (1994). Numerische Untersuchung des Mischungsverhaltens von Filmkühlstrahlen in Turbinenströmungen. *Doctoral Thesis,* Ruhr-Universität Bochum, Germany.

(14) Berg, H.P., Hennecke, D.K., Elfert, M., Hein, O. (1991). The Effect of Rotation on Local Coolant Side Flow and Heat Transfer in Turbine Blades. *Proc. of the 10th Int. Symp. on Air Breathing Engines (X.ISABE),* Nottingham, UK, Sept. 1991, 170-183. Also: *ISABE* Paper 91-7016.

(15) Elfert, M. (1993). The Effect of Rotation and Buoyancy on Flow Development in a Rotating Circular Coolant Channel. *Proc. of the 2nd Int. Symp. on Eng. Turbulence Modelling and Measurements,* 815-824, Elsevier, New York.

(16) Elfert, M. (1994). The Effect of Rotation and Buoyancy on Flow Development in a Rotating Circular Coolant Channel With Radial Inward Flow. in: Measurements in Turbulent Flows. *Experimental Thermal and Fluid Science (ETFS) Journal,* Special issue.

(17) Elfert, M. (1994). The Effect of Rotation and Buoyancy on Radially Inward and Outward Directed Flow in a Rotating Circular Coolant Channel. *49th ATI Congress of Thermotechnic Association of Italy,* 26-30 Sept., Perugia, Italy, Proceedings, 2375-2387.

(18) Schodl, R. (1989). Measurement Techniques in Aerodynamics. *VKI Lecture Series 1989-05,* Von Karman Institute , Brussels, Belgium.

(19) Schodl, R. (1986). Laser-two-focus Velocimetry. in: *Advanced Instrumentation for Aero Engine Components,* AGARD-CP-399, paper 7, Philadelphia, USA.

(20) Beversdorff, M., Hein, O., Schodl, R.. (1992). An L2F-Measurement Device with Image Rotator Prism for Flow Velocity Analysis in Rotating Coolant Channels. *80th Symp.on Heat Transfer and Cooling in Gas Turbines,* AGARD PEP, Antalya, Turkey.

(21) Schodl, R. (1977). Entwicklung des Laser-Zwei-Fokus-Verfahrens für die berührungslose Messung der Strömungsvektoren, insbesondere in Turbomaschinen. *Ph.D.Thesis,* Tech. Univ. Aachen, Germany.

(22) Chorin, A.J. (1967). A Numerical Method for Solving Incompressible Viscous Flow Problems. *Journal of computational Physics*, **2**, 12-26..